

# Estimation of time-varying transmission and removal rates underlying epidemiological processes: a new statistical tool for the COVID-19 pandemic

Hyokyoung G. Hong<sup>1,2</sup> and Yi Li<sup>3\*</sup>,

**1** Department of Statistics and Probability, Michigan State University, East Lansing, MI, USA

**2** Institute for Health Policy, Michigan State University, East Lansing, MI, USA

**3** Department of Biostatistics, University of Michigan, Ann Arbor, MI, USA

\* yili@umich.edu

## Abstract

The coronavirus pandemic has rapidly evolved into an unprecedented crisis. The susceptible-infectious-removed (SIR) model and its variants have been used for modeling the pandemic. However, time-independent parameters in the classical models may not capture the dynamic transmission and removal processes, governed by virus containment strategies taken at various phases of the epidemic. Moreover, very few models account for possible inaccuracies of the reported cases. We propose a Poisson model with time-dependent transmission and removal rates to account for possible random errors in reporting and estimate a time-dependent disease reproduction number, which may be used to assess the effectiveness of virus control strategies. We apply our method to study the pandemic in several severely impacted countries, and analyze and forecast the evolving spread of the coronavirus. We have developed an interactive web application to facilitate readers' use of our method.

## 1 Introduction

Coronaviruses are enveloped single-stranded positive-sense RNA viruses belonging to a broad family of coronaviridae and are widely harbored in animals [1–3]. Most of the coronaviruses only cause mild respiratory infections, but SARS-CoV-2, a newly identified member of the coronavirus family, initiated the very contagious and lethal coronavirus disease 2019 (COVID-19) in December 2019 [4, 5]. Since the detection of the first case in Wuhan, the COVID-19 pandemic has evolved into a global crisis within only four months. As of 4/9/2020, the virus has infected about 1.6 million individuals, caused more than 100,000 deaths [6], and altered the life of billions of people.

The pandemic has been closely monitored by the international society. Since 1/22/2020, daily numbers of infectious and recovered cases, and deaths have been reported for nearly every country. Much effort has been devoted by the affected countries to battling the disease. However, the crisis has yet been mitigated, with new infections detected every day. To forecast when the pandemic gets controlled, it is imperative to develop appropriate models to describe and understand the change trend of the pandemic [7–10].

The susceptible-infectious-removed (SIR) model was utilized to explain the rapid rise and fall of the infected individuals from the epidemics of severe acute respiratory syndrome (SARS), influenza A virus subtype (H1N1) and middle east respiratory syndrome (MERS) [11–15]. The key idea is to divide a total population into three compartments: the susceptible,  $S$ , who are healthy individuals capable of contracting the disease; the infectious,  $I$ , who have the disease and are infectious; and the removed,  $R$ , who have recovered from the disease and gained immunity or who have died from the disease [16]. The model assumes a one-way flow from susceptible to infectious to removed, and is reasonable for infectious diseases, which are transmitted from human to human, and where recovery confers lasting resistance [17].

SIR models originated from the Kermack-McKendrick model [18], consisting of three coupled differential equations to describe the dynamics of the numbers in the  $S, I$  and  $R$  compartments, which tend to fluctuate over time. For example, the number of infectious individuals increases drastically at the start of the epidemic, with a surge in susceptible individuals becoming infectious. As the epidemic develops, the number of infectious individuals decreases when more infectious individuals die or recover than susceptible individuals become infectious. The epidemic ends when the infectious compartment ceases to exist [16, 18].

SIR models and the modified versions, such as susceptible-exposed-infectious-recovered model (SEIR), were applied to analyze the COVID-19 outbreak [19–23]. Many of these models assume constant transmission and removal rates, which may not hold in reality. For example, as a result of various virus containment strategies, such as self-quarantine and social distancing mandates, the transmission and removal rates may vary over time [24]. Recently, [25–27] considered time-dependent SIR models adapted to the dynamical epidemiological processes evolving over time. However, very few considered random errors in reporting, such as under-reporting (e.g. asymptomatic cases or virus mutation) or over-reporting (e.g. false positives of testing), or characterized the uncertainty of predictions.

Poisson models naturally fit count data [28]. Several works [29–31] used Poisson distributions to model  $I$  and  $R$  from frequentist or Bayesian perspectives; however, most of the works only considered constant transmission and removal rates. How to extend these works to accommodate time-dependent rates remains elusive.

We propose to adopt a Poisson model to estimate the time-varying transmission and removal rates, and understand the trends of the pandemic across countries. For example, we can predict the number of the infectious persons and the number of removed persons at a certain time for each country, and forecast when the curves of cases become flattened.

An important epidemiologic index that characterizes the transmission potential is the basic reproduction number,  $\mathcal{R}_0$ , defined as the expected number of secondary cases produced by an infectious case [32–34]. Our model leads to a temporally dynamical  $\mathcal{R}_0$ , which measures at a given time how many people one infectious person, during the infectious period, will infect [35]. This may help evaluate the quarantine policies implemented by various authorities. A recent work [35] demonstrated that  $\mathcal{R}_0$  is likely to vary “due to the impact of the performed intervention strategies and behavioral changes in the population.”

The merits of our work are summarized as follows. First, unlike the deterministic ODE-based SIR models, our method does not require transmission and removal rates to be known, but estimates them using the data. Second, we allow these rates to be time-varying. Some time-varying SIR approaches [27] directly integrated into the model the information on when governments enforced, for example, quarantine, social-distancing, compulsory mask-wearing and city lockdowns. We differ by computing a time-varying  $\mathcal{R}_0$ , which gauges the status of coronavirus containment and assesses the effectiveness of virus control strategies. Third, our Poisson model accounts for possible random errors in reporting (such as false positives and false negatives of infectious cases), and quantifies the uncertainty of the predicted numbers of susceptible, infectious and removed. Finally, we have developed an interactive web application which facilitates readers’ use of our method.

## 2 A Poisson model with time-dependent transmission and removal rates

We introduce a Poisson model with time-varying transmission and removal rates, denoted by  $\beta(t)$  and  $\gamma(t)$ . Consider a population with  $N$  individuals, and denote by  $S(t), I(t), R(t)$  the true but unknown numbers of susceptible, infectious and removed, respectively, at time  $t$ , and by  $s(t) = S(t)/N$ ,  $i(t) = I(t)/N$ ,  $r(t) = R(t)/N$  the fractions of these compartments.

## 2.1 Time-varying transmission, removal rates and reproduction number

The following ordinary differential equations (ODE) describe the change rates of  $s(t)$ ,  $i(t)$  and  $r(t)$ :

$$\begin{aligned}\frac{ds(t)}{dt} &= -\beta(t)s(t)i(t), \\ \frac{di(t)}{dt} &= \beta(t)s(t)i(t) - \gamma(t)i(t), \\ \frac{dr(t)}{dt} &= \gamma(t)i(t),\end{aligned}\tag{1}$$

with an initial condition:  $i(0) = i_0$  and  $r(0) = r_0$ , where  $i_0 > 0$  in order to let the epidemic develop [36]. Here,  $\beta(t) > 0$  is the time-varying transmission rate of an infection at time  $t$ , which is the number of infectious contacts that result in infections per unit time, and  $\gamma(t) > 0$  is the time-varying removal rate at  $t$ , at which infectious subjects are removed from being infectious due to death or recovery [33]. Moreover,  $\gamma^{-1}(t)$  can be interpreted as the infectious duration of an infection caught at time  $t$  [37].

From (1), we derive an important quantity, which is the time-dependent reproduction number

$$\mathcal{R}_0(t) = \frac{\beta(t)}{\gamma(t)}.$$

Indeed, dividing the second equation by the third equation in (1) leads to

$$\mathcal{R}_0(t) = \frac{1}{s(t)} \left\{ \frac{di}{dr}(t) + 1 \right\},\tag{2}$$

where  $(di/dr)(t)$  is the ratio of the change rate of  $i(t)$  to that of  $r(t)$ . Therefore, compared to its time-independent counterpart,  $\mathcal{R}_0(t)$  is an instantaneous reproduction number and provides a real-time picture of an outbreak. For example, at the onset of the outbreak and in the absence of any containment actions, we may see a rapid ramp-up of cases compared to those removed, leading to a large  $(di/dr)(t)$  in (2), and hence a large  $\mathcal{R}_0(t)$ . With the implemented policies for disease mitigation, we will see a drastically decreasing  $(di/dr)(t)$  and, therefore, declining of  $\mathcal{R}_0(t)$  over time. The turning point is  $t_0$  such that  $\mathcal{R}_0(t_0) = 1$ , when the outbreak is controlled with  $(di/dr)(t_0) < 0$ .

Under the fixed population size assumption, i.e.,  $s(t) + i(t) + r(t) = 1$ , we only need to study  $i(t)$  and  $r(t)$ , and re-express (1) as

$$\begin{aligned}\frac{di(t)}{dt} &= \beta(t)i(t)\{1 - i(t) - r(t)\} - \gamma(t)i(t), \\ \frac{dr(t)}{dt} &= \gamma(t)i(t),\end{aligned}\tag{3}$$

with the same initial condition.

## 2.2 A Poisson model based on discrete time-varying SIR

As the numbers of cases and removed are reported on a daily basis,  $t$  is measured in days, e.g.  $t = 1, \dots, T$ . Replacing derivatives in (3) with finite differences, we can consider a discrete version of (3):

$$\begin{aligned}i(t+1) - i(t) &= \beta(t)i(t)\{1 - i(t) - r(t)\} - \gamma(t)i(t), \\ r(t+1) - r(t) &= \gamma(t)i(t),\end{aligned}\tag{4}$$

where  $\beta(t)$  and  $\gamma(t)$  are positive functions of  $t$ . We set  $i(1) = i_0 > 0$  and  $r(1) = r_0$ , with  $t = 1$  being the starting date.

We assume that  $s(t) \doteq 1$ , or  $i(t) + r(t) \doteq 0$ , for  $t = 1, \dots, T$ , that is, the portion of the infectious and removed is minor compared to the susceptible in a general population. This seems true before

the pandemic infects a sizable portion of the population. For example, even in the countries severely attacked, such as Italy, the US and Spain,  $s(t) > 99.5\%$  as of 4/9/2020 [6]. We then propose a modified version of (4):

$$\begin{aligned} i(t+1) - i(t) &= \beta(t)i(t) - \gamma(t)i(t), \\ r(t+1) - r(t) &= \gamma(t)i(t). \end{aligned} \quad (5)$$

As the first equation of (5) implies  $i(t+1) = \{1 + \beta(t) - \gamma(t)\}i(t)$ , (5) admits a “closed-form” solution:

$$\begin{aligned} i(t) &= i_0 \prod_{j=1}^{t-1} \{1 + \beta(j) - \gamma(j)\}, \\ r(t) &= \sum_{j=1}^{t-1} \gamma(j)i(j) + r_0 \end{aligned} \quad (6)$$

for  $t = 2, \dots, T$ . Equation (6) implies that when  $\mathcal{R}_0(t) = \beta(t)\gamma^{-1}(t) < 1$ ,  $i(t+1) < i(t)$  or the number of infectious cases drops, meaning the spread of virus is controlled; otherwise, the number of infectious cases will keep increasing.

### 2.3 Estimation and inference

Nonparametric techniques, such as splines [38], local polynomial regression [39] and reproducible kernel Hilbert space method [40], can be used to model  $\beta(t)$  and  $\gamma(t)$ . Based on our numerical experiences, however, simple polynomial approximations can work well. In particular, we specify

$$\begin{aligned} \log \beta(t) &= \beta_0 + \beta_1(t/C_0) + \dots + \beta_p(t/C_0)^p, \\ \log \gamma(t) &= \gamma_0 + \gamma_1(t/C_0) + \dots + \gamma_q(t/C_0)^q, \end{aligned} \quad (7)$$

where  $C_0$  is a large constant relative to  $T$  (e.g.  $2T$ ) to enhance numerical stability. As such, the polynomials can be regarded as truncated Taylor expansions of  $\log \beta(t)$  and  $\log \gamma(t)$  around 0. As  $p$  and  $q$  are unknown, we can choose them by using the Akaike information criterion (AIC) or the Bayesian information criterion (BIC). When  $p = q = 0$ , the model reduces to a constant SIR model.

Denote by  $\boldsymbol{\beta} = (\beta_0, \dots, \beta_p)$  and  $\boldsymbol{\gamma} = (\gamma_0, \dots, \gamma_q)$  the unknown parameters, by  $Z_I(t)$  and  $Z_R(t)$  the reported numbers of infectious and removed, respectively, and by  $z_I(t) = Z_I(t)/N$  and  $z_R(t) = Z_R(t)/N$ , the reported proportions. Also, denote by  $I(t)$  and  $R(t)$  the true numbers of infectious and removed, respectively at time  $t$ . We propose a Poisson model to link  $Z_I(t)$  and  $Z_R(t)$  to  $I(t)$  and  $R(t)$  as follows:

$$Z_R(t) \sim \text{Pois}(R(t)) \text{ and } Z_I(t) \sim \text{Pois}(I(t)). \quad (8)$$

We also assume that, given  $I(t)$  and  $R(t)$ , the observed  $(Z_I(t), Z_R(t))$  are independent across  $t = 1, \dots, T$ , meaning the random reporting errors are “white” noise.

With (5), (6) and (7),  $R(t)$  and  $I(t)$  are the functions of  $\boldsymbol{\beta}$  and  $\boldsymbol{\gamma}$ , since  $R(t) = N \times r(t)$  and  $I(t) = N \times i(t)$ . Given the data  $(Z_I(t), Z_R(t)), t = 1, \dots, T$ , we obtain  $(\hat{\boldsymbol{\beta}}, \hat{\boldsymbol{\gamma}})$ , the estimates of  $(\boldsymbol{\beta}, \boldsymbol{\gamma})$ , by maximizing the likelihood

$$L(\boldsymbol{\beta}, \boldsymbol{\gamma}) = \prod_{t=1}^T \frac{e^{-R(t)} R(t)^{Z_R(t)}}{Z_R(t)!} \times \prod_{t=1}^T \frac{e^{-I(t)} I(t)^{Z_I(t)}}{Z_I(t)!},$$

or, equivalently, maximizing the log likelihood function

$$\ell(\boldsymbol{\beta}, \boldsymbol{\gamma}) = N \sum_{t=1}^T \{-r(t) + z_R(t) \log r(t) - i(t) + z_I(t) \log i(t)\} + C, \quad (9)$$

where  $C$  is a constant free of  $\beta$  and  $\gamma$ . To solve this optimization problem, we differentiate  $\ell(\beta, \gamma)$  with respect to  $(\beta, \gamma)$ . Then  $(\hat{\beta}, \hat{\gamma})$  solves the following estimating equations:

$$\begin{aligned}\sum_{t=2}^T \left[ \left\{ \frac{z_R(t)}{r(t)} - 1 \right\} \frac{\partial}{\partial \beta} r(t) + \left\{ \frac{z_I(t)}{i(t)} - 1 \right\} \frac{\partial}{\partial \beta} i(t) \right] &= 0, \\ \sum_{t=2}^T \left[ \left\{ \frac{z_R(t)}{r(t)} - 1 \right\} \frac{\partial}{\partial \gamma} r(t) + \left\{ \frac{z_I(t)}{i(t)} - 1 \right\} \frac{\partial}{\partial \gamma} i(t) \right] &= 0,\end{aligned}$$

where the summation starts from  $t = 2$  as the term corresponding to  $t = 1$  is 0 by using the initial condition and, for  $t \geq 2$ ,

$$\begin{aligned}\frac{\partial}{\partial \beta} i(t) &= i(t) \sum_{j=1}^{t-1} \frac{\frac{\partial}{\partial \beta} \beta(j)}{1 + \beta(j) - \gamma(j)}, \\ \frac{\partial}{\partial \gamma} i(t) &= -i(t) \sum_{j=1}^{t-1} \frac{\frac{\partial}{\partial \gamma} \gamma(j)}{1 + \beta(j) - \gamma(j)}, \\ \frac{\partial}{\partial \beta} r(t) &= \sum_{j=1}^{t-1} \gamma(j) \frac{\partial}{\partial \beta} i(j), \\ \frac{\partial}{\partial \gamma} r(t) &= \sum_{j=1}^{t-1} \gamma(j) \frac{\partial}{\partial \gamma} i(j) + \sum_{j=1}^{t-1} i(j) \frac{\partial}{\partial \gamma} \gamma(j).\end{aligned}$$

Here,  $\frac{\partial}{\partial \beta} \beta(j) = \beta(j) \times (1, j/C_0, \dots, (j/C_0)^p)^\top$  and  $\frac{\partial}{\partial \gamma} \gamma(j) = \gamma(j) \times (1, j/C_0, \dots, (j/C_0)^q)^\top$ .

We then estimate the variance-covariance matrix of  $(\hat{\beta}, \hat{\gamma})$  by inverting the second derivative of  $-\ell(\beta, \gamma)$  evaluated at  $(\hat{\beta}, \hat{\gamma})$ . Finally, for  $t = 1, \dots, T$ , we estimate  $I(t)$  and  $R(t)$  by  $\hat{I}(t) = N\hat{i}(t)$  and  $\hat{R}(t) = N\hat{r}(t)$ , where  $\hat{i}(t)$  and  $\hat{r}(t)$  are obtained from (6) with all unknown quantities replaced by their estimates; estimate  $\beta(t)$  and  $\gamma(t)$  by  $\hat{\beta}(t)$  and  $\hat{\gamma}(t)$ , obtained by using (7) with  $(\beta, \gamma)$  replaced by  $(\hat{\beta}, \hat{\gamma})$ ; and estimate  $\mathcal{R}_0(t)$  by  $\hat{\mathcal{R}}_0(t) = \hat{\beta}(t)/\hat{\gamma}(t)$ .

---

#### Summary of estimation and inference for $\beta(t)$ , $\gamma(t)$ , $\mathcal{R}_0(t)$ , $I(t)$ , $R(t)$

---

**Estimation:** Let  $N$  be the size of population of a given country. The date when the first case was reported is set to be the starting date with  $t = 1$ ,  $i_0 = Z_I(1)/N$  and  $r_0 = Z_R(1)/N$ . The observed data are  $\{Z_I(t), Z_R(t), t = 1, \dots, T\}$ .

**Selection of  $p$ :** In (7), we set  $p = q$  in practice for computational convenience and maximize (9) to obtain  $\hat{\beta} = (\hat{\beta}_0, \hat{\beta}_1, \dots, \hat{\beta}_p)$  and  $\hat{\gamma} = (\hat{\gamma}_0, \hat{\gamma}_1, \dots, \hat{\gamma}_p)$ . The optimal  $p$ , denoted by  $p^*$ , minimizes the AIC or BIC criterion:

$$\begin{aligned}\text{AIC}(p) &= -2\ell(\hat{\beta}, \hat{\gamma}) + 4(p + 1), \\ \text{BIC}(p) &= -2\ell(\hat{\beta}, \hat{\gamma}) + 2 \log(T)(p + 1).\end{aligned}$$

When there is no confusion, in the following we denote by  $\hat{\beta} = (\hat{\beta}_0, \hat{\beta}_1, \dots, \hat{\beta}_{p^*})$  and  $\hat{\gamma} = (\hat{\gamma}_0, \hat{\gamma}_1, \dots, \hat{\gamma}_{p^*})$ . We also calculate  $\hat{\beta}(t)$ ,  $\hat{\gamma}(t)$ ,  $\hat{\mathcal{R}}_0(t)$ ,  $\hat{R}(t)$ ,  $\hat{I}(t)$  with  $p = p^*$ .

**Inference:** The estimated variance-covariance matrix of  $(\hat{\beta}, \hat{\gamma})$ , denoted by  $\hat{V}(\hat{\beta}, \hat{\gamma})$ , is obtained by inverting the second derivative of  $-\ell(\beta, \gamma)$  evaluated at  $(\hat{\beta}, \hat{\gamma})$ . For each  $t$ , as  $\hat{\beta}(t)$ ,  $\hat{\gamma}(t)$ ,  $\hat{\mathcal{R}}_0(t)$ ,  $\hat{R}(t)$  and  $\hat{I}(t)$  are smooth functions of  $\hat{\beta}$  and  $\hat{\gamma}$ , we apply the delta method [41] to estimate their variances and obtain the confidence intervals. As an illustration, we compute  $\widehat{\text{var}}(\hat{R}(t)) = \dot{R}(t)^\top \hat{V}(\hat{\beta}, \hat{\gamma}) \dot{R}(t)$  and  $\widehat{\text{var}}(\hat{I}(t)) = \dot{I}(t)^\top \hat{V}(\hat{\beta}, \hat{\gamma}) \dot{I}(t)$ , where  $\dot{R}(t)$  and  $\dot{I}(t)$  are the partial derivative vectors of  $\hat{R}(t)$  and  $\hat{I}(t)$  with respect to  $(\hat{\beta}, \hat{\gamma})$ .

---

### 3 Monte Carlo simulations

#### 3.1 Effects of mis-specifications of $i_0$ and $r_0$ on estimation

An important question to address is what roles the initial values  $r_0$  and  $i_0$  play in estimation. Accurate assessment of  $i_0$  can be problematic as in the beginning of an epidemic, cases are likely to be under-reported or unreported because of lack of awareness or lack of testing. For a deterministic SIR model (5),  $r(t)$  and  $i(t)$  may heavily depend on their initial values. As shown in Figure 1, when the initial value  $i_0$  is mis-specified to be 5 times of the truth, the curves of  $i(t)$  and  $r(t)$  are biased to the left. On the other hand, our proposed statistical model (8), by accounting for the randomness of the observed data, is more robust toward the mis-specification of  $i_0$  and  $r_0$ , and estimates  $r(t)$  and  $i(t)$  with negligible biases even with mis-specified initial values. We also mis-specify  $i_0$  to be only twice of the truth, and obtain the same results, which are omitted.

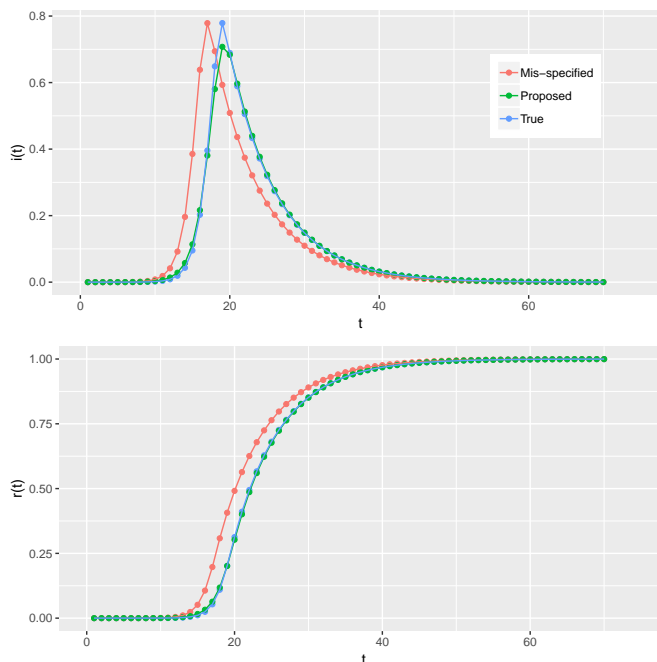


**Fig 1.** Plots of the  $i(t)$  (upper) and  $r(t)$  (lower) based on the deterministic SIR model (5) with true initials (“True”), and with the mis-specified initials (“Mis-specified”), and the estimated  $i(t)$  and  $r(t)$  using the proposed model (8) with the mis-specified initials (“Proposed”). The  $i(t)$  and  $r(t)$  are generated using  $(\beta, \gamma) = (e^{0.35}, e^{-1.95})$  and  $(i_0, r_0) = (10^{-6}, 10^{-6})$  in (5). The mis-specified initials are  $(5 \times 10^{-6}, 5 \times 10^{-6})$ .

#### 3.2 Sensitivity analysis

We explore the robustness of the estimates of  $r(t)$  and  $i(t)$  when  $\beta(t)$  and  $\gamma(t)$  are mis-specified. We generate  $Z_R(t)$  and  $Z_I(t)$  with Model (8), where  $R(t)$  and  $I(t)$  are specified by the SIR model (5) with  $r_0 = i_0 = 10^{-6}$ ,  $\beta(t) = 1 - 0.005t$  and  $\gamma(t) = 0.5 + 0.002t$ , for  $t = 1, \dots, 70$ . A total of 1,000 datasets are generated. We apply the proposed method to analyze each dataset and estimate  $i(t)$  and  $r(t)$  for  $t = 1, \dots, 70$ . Figure 2 examines the relative biases of the estimates of  $i(t)$ ,  $r(t)$  and  $\mathcal{R}_0(t)$  at each  $t$ . In the first few days of the time series,  $i(t)$  and  $r(t)$  are overestimated, but as  $t$  gets large the biases become negligible. On the other hand, the estimates of  $\mathcal{R}_0(t)$  incur few biases. All suggest the robustness of our method.

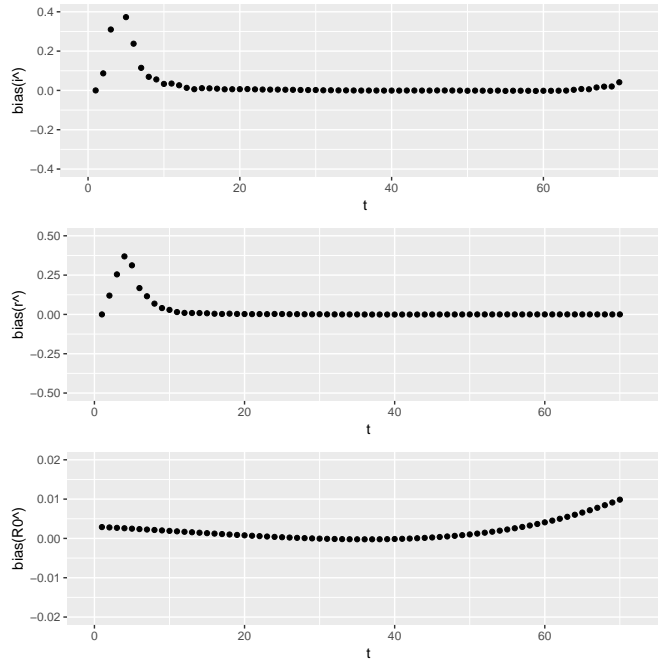


**Fig 2.** Sensitivity analysis on the estimation of  $i(t)$  (top),  $r(t)$  (middle), and  $\mathcal{R}_0(t)$  (bottom) when  $\beta(t)$  and  $\gamma(t)$  are mis-specified. The relative biases are drawn against  $t$ , where the relative bias is defined as the bias divided by the true value. Results are the averages over 1,000 independent datasets.

### 3.3 Choice of $p$ and estimation of $\beta$ and $\gamma$

**Example 1.** With a constant SIR model, we investigate whether the AIC or BIC criterion chooses the correct order of polynomial ( $p = 0$ ), and compare  $\hat{\beta}$  and  $\hat{\gamma}$  with the true  $\beta$  and  $\gamma$ . We generate 1,000 independent datasets with the following setting:  $i_0 = 10^{-6}$ ,  $r_0 = 0$ ,  $\beta = \exp(\beta_0)$ , and  $\gamma = \exp(\gamma_0)$ , where  $\beta_0 = 0.35$  and  $\gamma_0 = -1.95$ ,  $t = 1, \dots, 70$ . The observed infectious case,  $Z_I(t)$ , and removal case,  $Z_R(t)$ , are generated from model (8), where  $R(t)$  and  $I(t)$  are specified by (5). Both AIC and BIC, for the majority of times, choose 0 (884 out of 1,000 for AIC, 986 out of 1,000 for BIC) and only occasionally choose 1.

We evaluate the performance of the proposed model using the bias and the agreement between the empirical and model based standard errors, based on 1,000 independently simulated datasets. The estimates are nearly unbiased and the model based standard errors match with the empirical standard errors; see Table 1.

**Example 2.** We modify Example 1 by specifying the true  $\beta(t)$  and  $\gamma(t)$  to be time-dependent with  $\beta(t) = \exp(\beta_0 + \beta_1 t/C_0)$  and  $\gamma(t) = \exp(\gamma_0 + \gamma_1 t/C_0)$ , where  $\beta_0 = 0.35$ ,  $\beta_1 = 1.2$ ,  $\gamma_0 = -1.95$ ,  $\gamma_1 = 1.4$ ,  $C_0 = 140$ ,  $t = 1, \dots, 70$ .

We observe that both AIC and BIC choose  $p^* = 1$  with an accuracy of 100%, the estimates are with negligible biases, and the model based standard errors agree to the empirical standard errors; see Table 1.

## 4 Analysis of the COVID-19 pandemic among severely impacted countries

### 4.1 Data descriptions

The Johns Hopkins University's Coronavirus Resource Center [6] hosts the country level data. We derive the number of active COVID-19 cases,  $I(t)$ , and the cumulative number of combined recovered

**Table 1.** Simulation results. Empirical SE is the standard deviation of the 1,000 estimates.

Example		$\beta_0$	$\beta_1$	$\gamma_0$	$\gamma_1$
1	Empirical SE	$9.64 \times 10^{-5}$		$2.58 \times 10^{-4}$	
	Model-based SE	$9.33 \times 10^{-5}$		$2.63 \times 10^{-4}$	
	Bias	$1.41 \times 10^{-6}$		$5.79 \times 10^{-6}$	
2	Empirical SE	$1.00 \times 10^{-3}$	$1.68 \times 10^{-2}$	$1.62 \times 10^{-3}$	$9.53 \times 10^{-3}$
	Model-based SE	$1.02 \times 10^{-3}$	$1.70 \times 10^{-2}$	$1.62 \times 10^{-3}$	$9.56 \times 10^{-3}$
	Bias	$3.10 \times 10^{-4}$	$-4.93 \times 10^{-3}$	$3.82 \times 10^{-4}$	$-2.24 \times 10^{-3}$

and deaths,  $R(t)$ , on a daily basis. We apply our model to study the pandemic in some representative countries which have been severely hit, such as China, France, Italy, Iran, Spain, South Korea, the UK, and the US.

## 4.2 Estimation of country-specific time-independent transmission, removal rates and $\mathcal{R}_0$

We first fit the model with constant transmission and removal rates. Though the model may not fit the data well, the estimated transmission and removal rates can roughly be interpreted as the averages of time-varying transmission and removal rates over the period of the observation time, and may give a simple exposition of how the countries fared during this crisis so far.

As of 4/9/2020, the basic reproduction number  $\mathcal{R}_0$  has been computed for 17 severely impacted countries (Figure 3). Among them, the estimated  $\mathcal{R}_0$  ranges from 1.16 to 17.40, with an average of 5.7. Countries, such as China and Korea, which developed the virus outbreak early, have a relatively low  $\hat{\mathcal{R}}_0$  of 1.16 and 2.44, meaning the outbreak has been reasonably controlled. Other countries, such as India, the US and Brazil, which were hit hard by the pandemic recently, have seen a ramp-up in virus testing with more cases detected, and the estimated  $\mathcal{R}_0$  is alarmingly high with 8.99, 14.1 and 17.4, respectively. However, we caution that  $\mathcal{R}_0$  is sensitive to the observation period and should be interpreted within a timing context [42].

## 4.3 Estimation of country-specific time-dependent transmission, removal rates and $\mathcal{R}_0$

Since the first case of COVID-19 was detected in Wuhan, China, it quickly spread to nearly every part of the world [6]. COVID-19, conjectured to be more contagious than the previous SARS and H1N1 [43], has put great strain on healthcare systems worldwide, especially among the severely impacted countries [44]. We apply our method to assess the epidemiological processes of COVID-19 in some of these countries; see Figure 4 for the estimated country-specific transmission, removal rates, and  $\mathcal{R}_0(t)$ .

In January 2020, the transmission rate in China was high with a low removal rate and rapidly rising cases, resulting in a high  $\mathcal{R}_0$ . Because of extremely stringent mitigation policies such as city lockdown and mandatory mask-wearing implemented in the end of January, China brought its epidemic under control with a quickly dropping  $\mathcal{R}_0$  in February. On Feb 15,  $\mathcal{R}_0$  touched 1, or equivalently,  $\log \mathcal{R}_0$  crossed 0, indicating that China has contained the epidemic and more people removed from infectious status than those who became infectious.

Korea followed a similar pattern. The sudden outbreak with a massive cluster of more than 5,000 cases was linked to a minor Christian sect [45], which explains an extremely high  $\mathcal{R}_0$  in the early phase of the epidemic. Since then, Korea appeared to have greatly slowed its epidemic, likely due to expansive testing programs and extensive efforts to trace and isolate patients and their contacts [46]. Around 3/17/2020,  $\mathcal{R}_0$  dropped below 1.

Since the early March, the US has seen soaring infectious cases, and  $\mathcal{R}_0$  reached the peak around 3/10/2020. Around that time, the federal government and several states have issued mandatory or



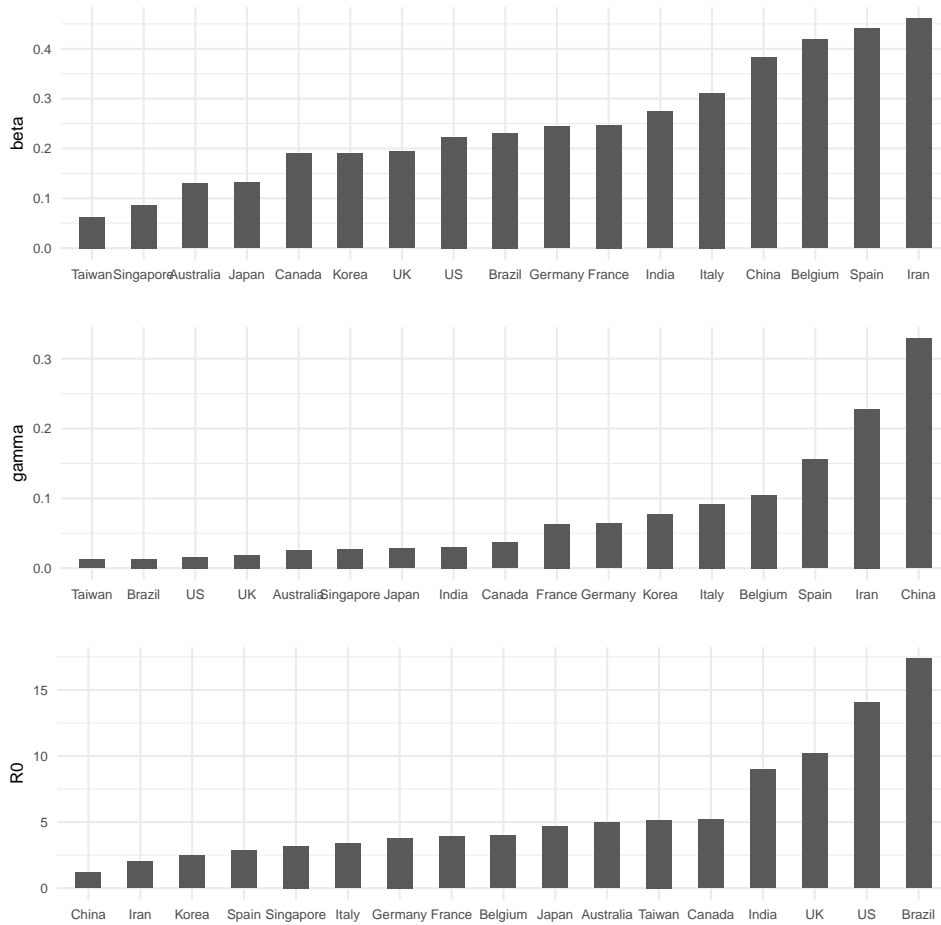


**Fig 3.** Estimates of  $\beta$ ,  $\gamma$ , and  $\mathcal{R}_0$  for model (5) with time-independent parameters, based on the data up to 4/9/2020.

advisory stay-home orders, which seemed to have lessened the virus spread. The transmission rate started decreasing around the mid-March and  $\mathcal{R}_0$  dropped from 38.04 on 3/10/2020 to 3.89 on 4/9/2020.

More broadly, Figure 4 categorizes countries into two groups based on the shape of  $\mathcal{R}_0$ . One group features a monotone decreasing  $\mathcal{R}_0$ . The countries, such as China and Korea, took aggressive actions after the outbreak and present sharper slopes of the curves. Some European countries, such as France, Iran, Italy and Spain, which were hit later than the Asian countries, share a similar pattern, though with much flatter slopes. On the other hand, bell-shaped curves are observed for the US and UK, likely because these governments were initially slow to react to the virus attack, but did take strong measures later to fight the disease. Nevertheless, almost all of the countries are featuring decreasing  $\mathcal{R}_0$ , which soon will likely drop below 1, and may be able to declare the containment of the epidemic in the near future.

Our model enables estimation of  $I(t)$  and  $R(t)$ . As an illustration, Figures 5 and 6 depict the estimated  $I(t)$  and  $R(t)$  curves for the selected countries. The red and green curves represent the observed data and the model-based predictions, respectively, with 95% confidence intervals. With a large  $N$ , the model-based standard errors are substantially small compared to  $\hat{I}(t)$  and  $\hat{R}(t)$ , making the confidence interval bounds hardly distinguished from  $\hat{I}(t)$  and  $\hat{R}(t)$ . The estimates of  $I(t)$  and  $R(t)$  seem to be fairly close to the observed numbers of infectious and removed cases, especially when the observed curves are smooth. As expected, larger prediction errors happen at where sudden jumps or drops occur. With extrapolations, our model can make reasonably accurate short-term predictions;

however, for long-term predictions, we are cautious as model-based predictions cannot reflect the consequences of the future policy changes.

We created an interactive web application (<https://youngchk.shinyapps.io/tvSIRforCOVID19/>) to facilitate users' application of the proposed method to compute the time-varying reproduction number, and to predict the daily numbers of active cases and removed cases for selected countries; see Figure 7 for an illustration.

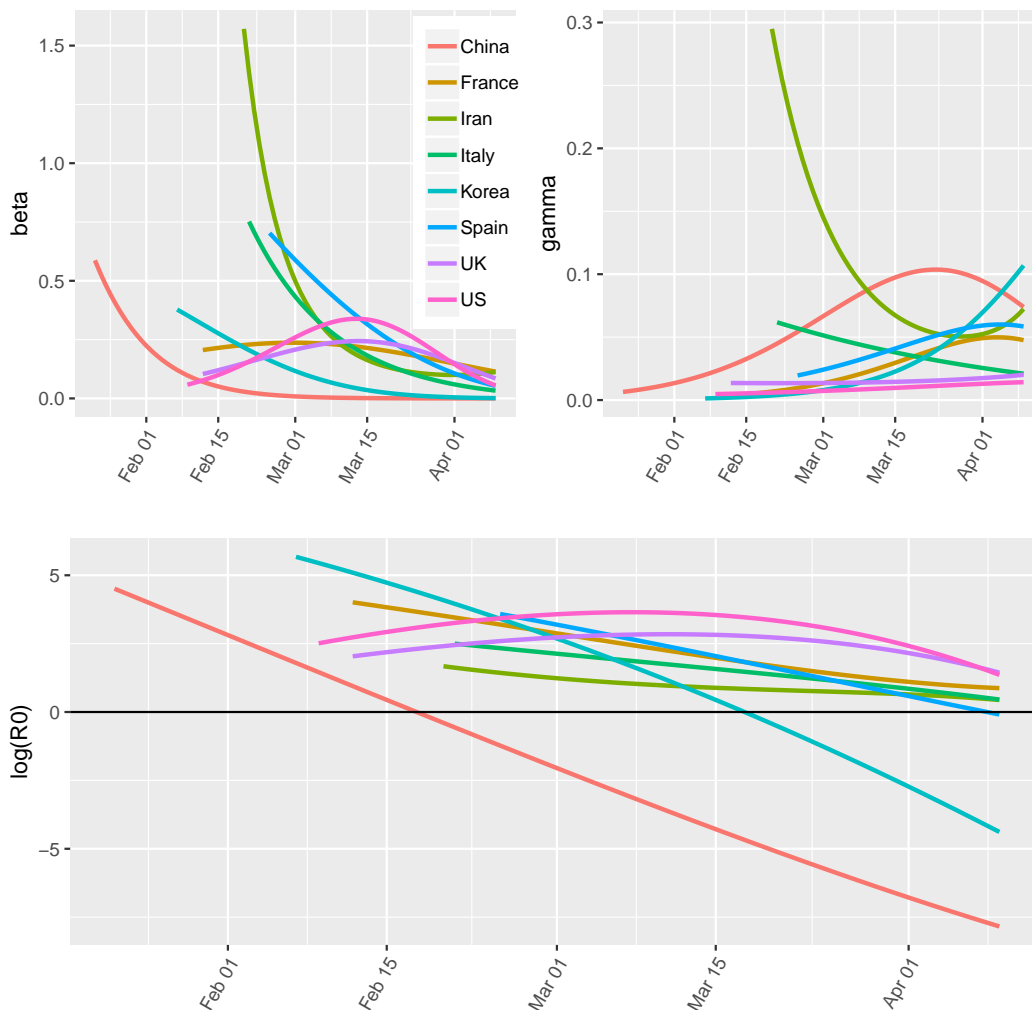


**Fig 4.** Estimated  $\beta(t)$ ,  $\gamma(t)$ , and  $\log \mathcal{R}_0(t)$ , based on the data up to 4/9/2020.

## Discussion

The rampaging pandemic of COVID-19 has called for developing proper computational and statistical tools to understand the trend of the spread of the disease and evaluate the efficacy of mitigation measures [47–50]. We propose a Poisson model with time-dependent transmission and removal rates. Our model accommodates possible random errors in the number reporting, and estimates a time-dependent disease reproduction number,  $\mathcal{R}_0(t)$ , which can serve as a metric for timely evaluating the effects of health policies. Applications of our method to study the epidemics in several selected countries illustrate the results of the virus containment policies implemented in these countries, and may serve as the epidemiological benchmarks for the future preventive measures.

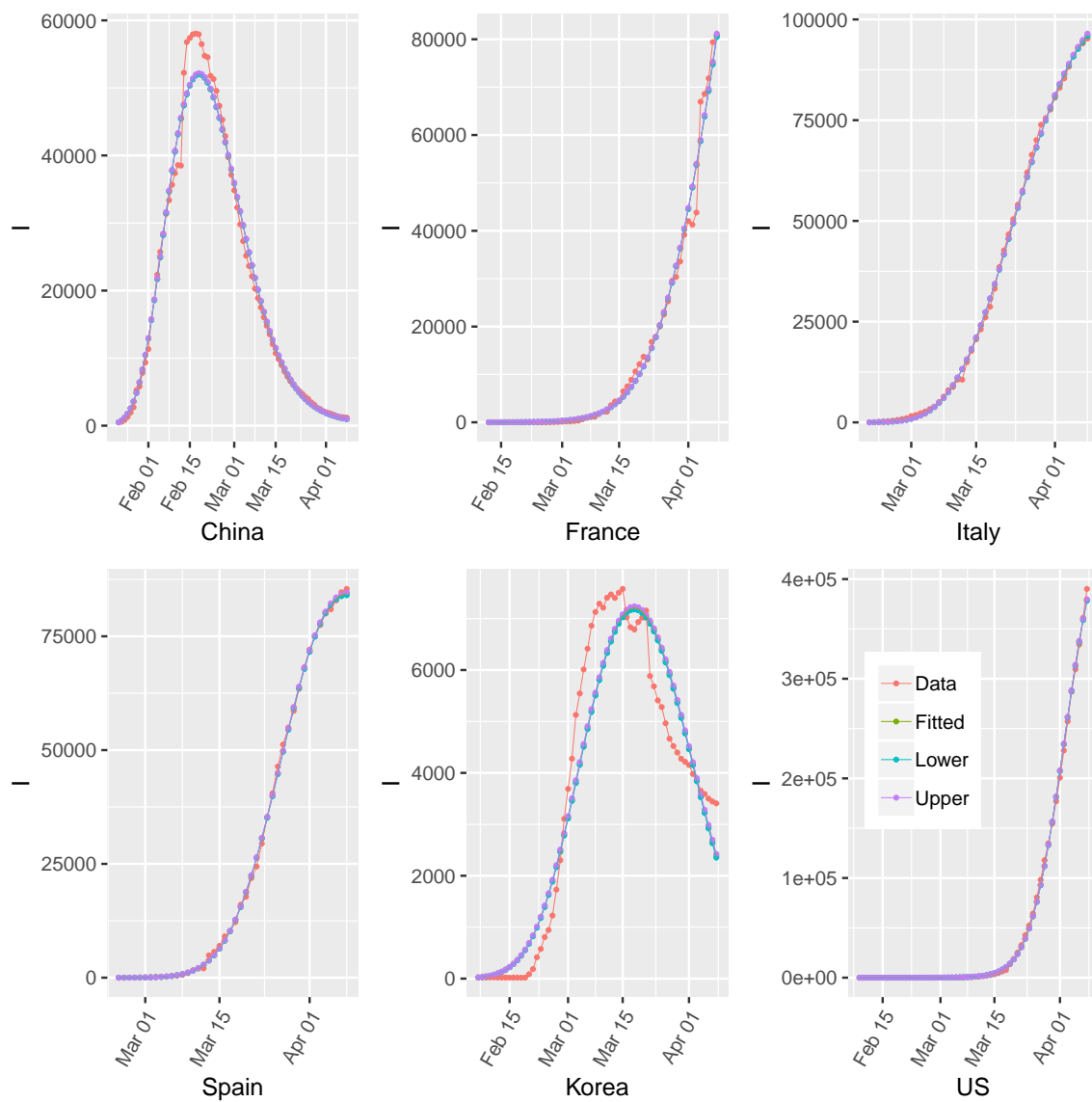


**Fig 5.** Estimated  $I(t)$  by countries, based on the data up to 4/9/2020.

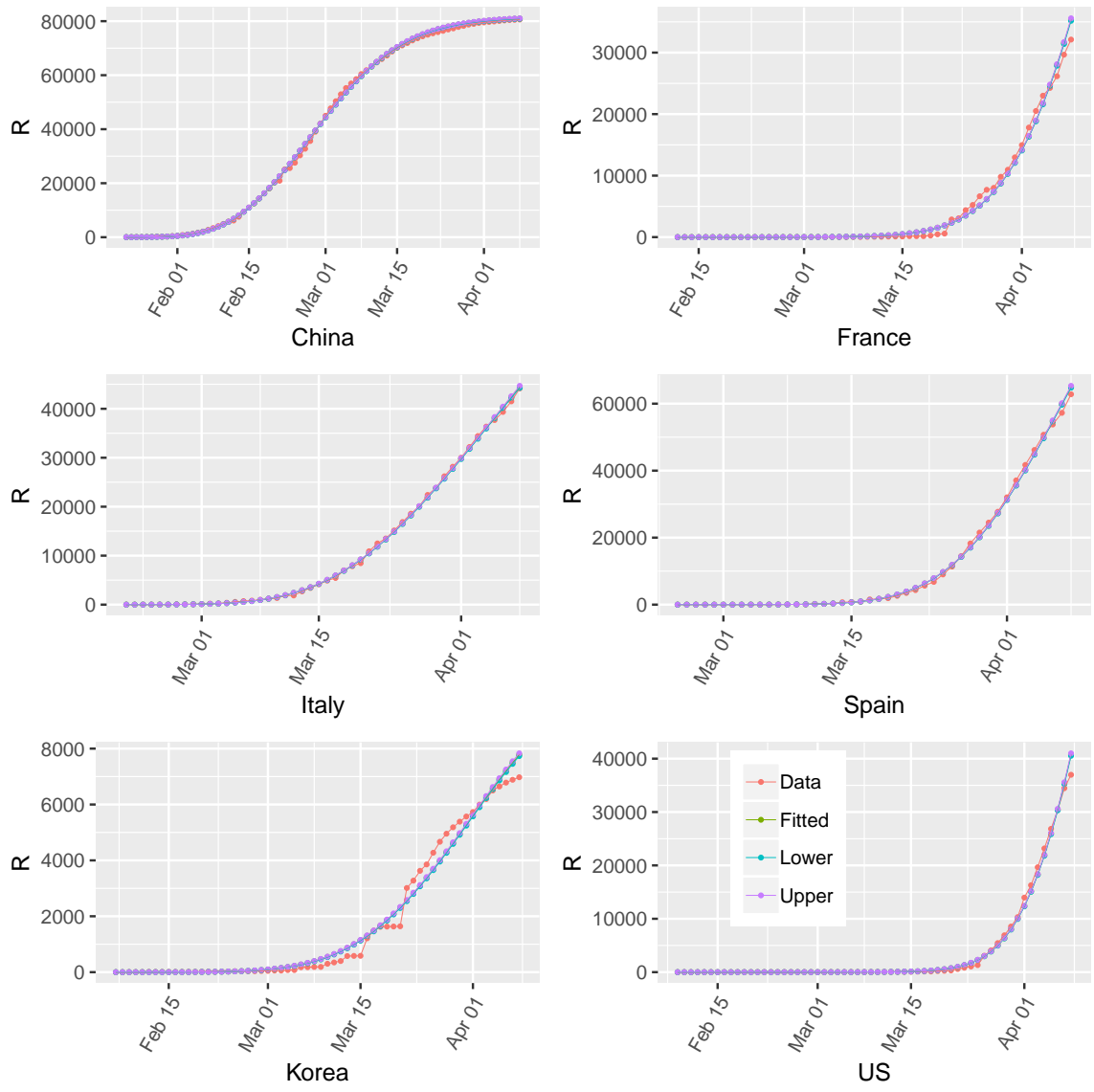


**Fig 6.** Estimated  $R(t)$  by countries, based on the data up to 4/9/2020.

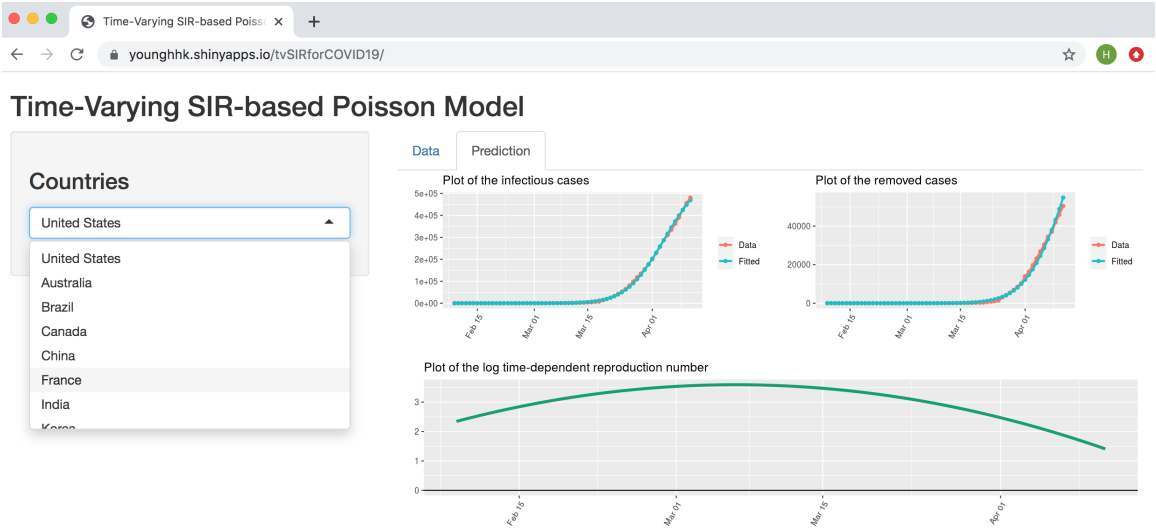


**Fig 7.** An illustration of the developed interactive web application.

Several methodological questions need to be addressed. First, we analyzed each country separately, without considering the traffic flows among these countries. We will develop a joint model for the global epidemic, which accounts for the geographic locations of and the connectivity among the countries. Second, we have ignored the birth and natural death processes (e.g. deaths due to non-COVID-19 causes), and also combined the recovered and deaths in our model. We will extend our model by considering them as separate compartments. Finally, to reduce the computational complexity, we have assumed that  $\log \beta(t)$  and  $\log \gamma(t)$  are polynomials and with the same order. Though the performance of our parametric approach is adequate, the model can be refined with more flexible functions or by using nonparametric approaches. In particular, model (5) implies

$$\mathcal{R}_0(t) = 1 + \frac{i(t+1) - i(t)}{r(t+1) - r(t)},$$

naturally leading to a nonparametric estimator

$$\widehat{\mathcal{R}}_0(t) = 1 + \frac{Z_I(t+1) - Z_I(t)}{Z_R(t+1) - Z_R(t)}.$$

We will pursue this.

## Conclusion

Containment of COVID-19 requires the concerted effort of health care workers, health policy makers as well as citizens. Measures, e.g. self-quarantine, social distancing, and shelter in place, have been executed at various phases by each country to prevent the community transmission. Timely and effective assessment of these actions constitutes a critical component of the effort. SIR models have been widely used to model this pandemic. However, constant transmission and removal rates may not capture the timely influences of these policies.

We propose a time-varying SIR Poisson model to assess the dynamic transmission patterns of COVID-19. With the virus containment measures taken at various time points,  $\mathcal{R}_0$  may vary substantially over time. Our model provides a systematic and daily updatable tool to evaluate the immediate outcomes of these actions. As some countries in Asia are now shifting gear to battle the second waves of virus attack induced by the imported cases [51, 52], our tool may also shed light on and aid the implementation of future containment strategies.

## Acknowledgments

This work was supported in part by the National Science Foundation and the National Institutes of Health.

## References

1. Fehr AR, Perlman S. Coronaviruses: an overview of their replication and pathogenesis. *Methods Mol Biol.* 2015;1282:1–23.
2. Li W, Shi Z, Yu M, Ren W, Smith C, Epstein JH, et al. Bats are natural reservoirs of SARS-like coronaviruses. *Science.* 2005;310(5748):676–679.
3. Woo PC, Lau SK, Lam CS, Lau CC, Tsang AK, Lau JH, et al. Discovery of seven novel Mammalian and avian coronaviruses in the genus deltacoronavirus supports bat coronaviruses as the gene source of alphacoronavirus and betacoronavirus and avian coronaviruses as the gene source of gammacoronavirus and deltacoronavirus. *Journal of Virology.* 2012;86(7):3995–4008.
4. Trombetta H, Faggion HZ, Leotte J, Nogueira MB, Vidal LR, Raboni SM. Human coronavirus and severe acute respiratory infection in Southern Brazil. *Pathogens and Global Health.* 2016;110(3):113–118.
5. Wang C, Liu L, Hao X, Guo H, Wang Q, Huang J, et al. Evolving epidemiology and impact of non-pharmaceutical interventions on the outbreak of coronavirus disease 2019 in Wuhan, China. 2020;doi:10.1101/2020.03.03.20030593.
6. Johns Hopkins Coronavirus Resource Center; 2020. Available from: <https://coronavirus.jhu.edu/>.
7. Hall I, Gani R, Hughes H, Leach S. Real-time epidemic forecasting for pandemic influenza. *Epidemiology & Infection.* 2007;135(3):372–385.
8. Grassly NC, Fraser C. Mathematical models of infectious disease transmission. *Nature Reviews Microbiology.* 2008;6(6):477–487.
9. Chang SL, Harding N, Zachreson C, Cliff OM, Prokopenko M. Modelling transmission and control of the COVID-19 pandemic in Australia. arXiv:2003.10218; 2020.
10. Pellis L, Scarabel F, Stage HB, Overton CE, Chappell LH, Lythgoe KA, et al. Challenges in control of Covid-19: short doubling time and long delay to effect of interventions. arXiv:2004.00117; 2020.
11. Laguzet L, Turinici G. Individual vaccination as Nash equilibrium in a SIR model with application to the 2009–2010 influenza A (H1N1) epidemic in France. *Bulletin of Mathematical Biology.* 2015;77(10):1955–1984.
12. Schwartz EJ, Choi B, Rempala GA. Estimating epidemic parameters: Application to H1N1 pandemic data. *Mathematical Biosciences.* 2015;270:198–203.
13. Huang X, Clements AC, Williams G, Mengersen K, Tong S, Hu W. Bayesian estimation of the dynamics of pandemic (H1N1) 2009 influenza transmission in Queensland: A space–time SIR-based model. *Environmental Research.* 2016;146:308–314.
14. Mkhathshwa T, Mummert A. Modeling super-spreading events for infectious diseases: case study SARS. arXiv:1007.0908; 2010.
15. Giraldo JO, Palacio DH. Deterministic SIR (Susceptible–Infected–Removed) models applied to varicella outbreaks. *Epidemiology & Infection.* 2008;136(5):679–687.

16. Blackwood JC, Childs LM. An introduction to compartmental modeling for the budding infectious disease modeler. *Letters in Biomathematics*. 2018;5(1):195–221.
17. Cox Jr LA. *Risk Analysis Foundations, Models, and Methods*. Springer Science & Business Media; 2012.
18. Kermack WO, McKendrick AG. A contribution to the mathematical theory of epidemics. *Proceedings of the Royal Society of London Series A*. 1927;115(772):700–721.
19. Nesteruk I. Statistics based predictions of coronavirus 2019-nCoV spreading in mainland China. medRxiv. 2020;doi:10.1101/2020.02.12.20021931.
20. Chen Y, Cheng J, Jiang Y, Liu K. A time delay dynamical model for outbreak of 2019-nCoV and the parameter identification. arXiv:2002.00418; 2020.
21. Peng L, Yang W, Zhang D, Zhuge C, Hong L. Epidemic analysis of COVID-19 in China by dynamical modeling. arXiv:2002.06563; 2020.
22. Zhou T, Liu Q, Yang Z, Liao J, Yang K, Bai W, et al. Preliminary prediction of the basic reproduction number of the Wuhan novel coronavirus 2019-nCoV. *Journal of Evidence-Based Medicine*; 2020.
23. Maier BF, Brockmann D. Effective containment explains sub-exponential growth in confirmed cases of recent COVID-19 outbreak in mainland China. arXiv:2002.07572; 2020.
24. Tognotti E. Lessons from the history of quarantine, from plague to influenza A. *Emerging Infectious Diseases*. 2013;19(2):254.
25. Chen YC, Lu PE, Chang CS, Liu TH. A Time-dependent SIR model for COVID-19 with undetectable infected persons. arXiv:2003.00122 [q-bio.PE]; 2020.
26. Boatto S, Bonnet C, Cazelles B, Mazenc F. SIR model with time dependent infectivity parameter : approximating the epidemic attractor and the importance of the initial phase; 2018. Available from: <https://hal.inria.fr/hal-01677886>.
27. Song PX, Wang L, Zhou Y, He J, Zhu B, Wang F, et al. An epidemiological forecast model and software assessing interventions on COVID-19 epidemic in China. medRxiv. 2020;doi:10.1101/2020.02.29.20029421.
28. Hilbe JM. *Modeling Count Data*. Cambridge University Press; 2014.
29. Kirkeby CT, Halasa T, Gussmann MK, Toft N, Græsbøll K. Methods for estimating disease transmission rates: Evaluating the precision of Poisson regression and two novel methods. *Scientific Reports*. 2018;8(1).
30. O’Dea EB, Pepin KM, Lopman BA, Wilke CO. Fitting outbreak models to data from many small norovirus outbreaks. *Epidemics*. 2014;6:18–29.
31. Zhuang L, Cressie N, Pomeroy L, Janies D. Multi-species SIR models from a dynamical Bayesian perspective. *Theoretical ecology*. 2013;6(4):457–473.
32. Dietz K. The estimation of the basic reproduction number for infectious diseases. *Statistical Methods in Medical Research*. 1993;2(1):23–41. doi:10.1177/096228029300200103.
33. Diekmann O, Heesterbeek JAP. *Mathematical Epidemiology of Infectious Diseases: Model Building, Analysis and Interpretation*. vol. 5. John Wiley & Sons; 2000.
34. Eichner M, Dietz K. Transmission potential of smallpox: estimates based on detailed data from an outbreak. *American Journal of Epidemiology*. 2003;158(2):110–117.

35. Liu QH, Ajelli M, Aleta A, Merler S, Moreno Y, Vespignani A. Measurability of the epidemic reproduction number in data-driven contact networks. *Proceedings of the National Academy of Sciences*. 2018;115(50):12680–12685.
36. Chen YC, Lu PE, Chang CS, Liu T. A Time-dependent SIR model for COVID-19 with undetectable infected persons. *arXiv preprint arXiv:200300122*. 2020;.
37. Jones H. Notes on  $R_0$ , Stanford University, Stanford; 2007.
38. De Boor C. *A Practical Guide to Splines*. vol. 27. Springer-Verlag New York; 1978.
39. Ruppert D. Empirical-bias bandwidths for local polynomial nonparametric regression and density estimation. *Journal of the American Statistical Association*. 1997;92(439):1049–1062.
40. Akgül A. New reproducing kernel functions. *Mathematical Problems in Engineering*; 2015.
41. Parr WC. A note on the jackknife, the bootstrap and the delta method estimators of bias and variance. *Biometrika*. 1983;70(3):719–722.
42. Delamater PL, Street EJ, Leslie TF, Yang YT, Jacobsen KH. Complexity of the basic reproduction number ( $R_0$ ). *Emerging Infectious Diseases*. 2019;25(1):1.
43. Sansonetti P. COVID-19, chronicle of an expected pandemic. *EMBO Molecular Medicine*. 2020;doi:<https://doi.org/10.15252/emmm.202012463>.
44. Tanne JH, Hayasaki E, Zastrow M, Pulla P, Smith P, Rada AG. Covid-19: how doctors and healthcare systems are tackling coronavirus worldwide. *BMJ*. 2020;368.
45. Yoon D, Martin TW. Why a South Korean church was the perfect petri dish for coronavirus; 2020 (accessed 03/02/20). Available from: <https://www.wsj.com/articles/why-a-south-korean-church-was-the-perfect-petri-dish-for-coronavirus-11583082110>.
46. Normile D. Coronavirus cases have dropped sharply in South Korea. What's the secret to its success?; 2020 (accessed 03/02/20). Available from: <https://www.sciencemag.org/news/2020/03/coronavirus-cases-have-dropped-sharply-south-korea-whats-secret-its-success>.
47. Hossain MM. Current status of global research on novel coronavirus disease (COVID-19): A bibliometric analysis and knowledge mapping; 2020.
48. Sarkodie SA, Owusu PA. Investigating the cases of novel coronavirus disease (COVID-19) in China using dynamic statistical techniques. *Heliyon*. 2020;6:e03747.
49. Zhang Y, Jiang B, Yuan J, Tao Y. The impact of social distancing and epicenter lockdown on the COVID-19 epidemic in mainland China: A data-driven SEIQR model study. *medRxiv*. 2020;doi:10.1101/2020.03.04.20031187.
50. Picchiotti N, Salvioli M, Zanardini E, Missale F. COVID-19 Italian and Europe epidemic evolution: A SEIR model with lockdown-dependent transmission rate based on Chinese data; 2020.
51. As China's virus cases reach zero, experts warn of second wave; 2020 (accessed 03/18/20). Available from: <https://www.bloomberg.com/news/articles/2020-03-18/as-china-virus-cases-near-zero-experts-warn-of-second-wave>.
52. Coronavirus: Asian nations face second wave of imported cases; 2020 (accessed 03/19/20). Available from: <https://www.bbc.com/news/world-asia-51955931>.